THE JOURNAL OF CHEMICAL PHYSICS **124**, 214901 (2006)

Mesoscopic description of solvent effects on polymer dynamics

Song Hi Lee[a)]
Department of Chemistry, Kyungsung University, Pusan 608-736, South Korea

Raymond Kapral[b)]
Chemical Physics Theory Group, Department of Chemistry, University of Toronto, Tonoto, ON M5S 3H6, Canada

(Received 31 January 2006; accepted 28 March 2006; published online 1 June 2006)

Solvent effects on polymer dynamics and structure are investigated using a mesoscopic solvent model that accounts for hydrodynamic interactions among the polymer beads. The simulation method combines molecular dynamics of the polymer chain, interacting with the solvent molecules through intermolecular forces, with mesoscopic multiparticle collision dynamics for the solvent molecules. Changes in the intermolecular forces between the polymer beads and mesoscopic solvent molecules are used to vary the solvent conditions from those for good to poor solvents. Polymer collapse and expansion dynamics following changes in solvent conditions are studied for homopolymer and block copolymer solutions. The frictional properties of polymers are also investigated. © *2006 American Institute of Physics*. [DOI: 10.1063/1.2198201]

I. INTRODUCTION

It is well known that the solvent plays an important role in determining the nature of polymer dynamics and polymer structure.[1–4] In good solvents the polymer exists in an expanded configuration while in poor solvent it adopts a compact form. If solution properties are suddenly changed from good to poor solvent conditions, polymer collapse will occur.[5] The collapse dynamics of polymers is akin to the early stages of folding transitions seen in proteins and this analogy has stimulated research in this area.

Polymer collapse dynamics has been intensively studied and a variety of models have been proposed for the mechanism of the collapse.[6–9] The existence of such a transition has been proven for exactly a solvable model of a polymer chain.[10] Simulations of model systems have been carried out to test these theoretical predictions. Polymer collapse dynamics is strongly influenced by the presence of hydrodynamic interactions among the polymer units due to coupling to collective solvent dynamical modes. Consequently, models have been based either on Langevin dynamics where solvent effects are included implicitly through frictional and random forces,[11–13] or on full molecular-dynamics simulations with explicit inclusion of solvent molecules.[14–16]

Frictional properties of polymers also depend strongly on solvent collective effects. Since polymer molecules are large, hydrodynamic interactions lead to Stokes-law-like forms for the friction and diffusion coefficients. The mesoscopic polymer lengths and complex shapes of polymers in solution, along with the presence of hydrodynamic interactions, make the computation of these frictional properties difficult. Most often simple macroscopic models are used to estimate their values.[1]

Full molecular-dynamics (MD) simulations on large polymers that include solvent molecules explicitly provide the most detailed information on polymer solution dynamics. Such simulations are lengthy and this places restrictions on the system size and accessible time scales. In this paper we examine some aspects of polymer dynamics and structure by carrying out simulations of a single polymer chain in a mesoscopic solvent evolving through multiparticle collision (MPC) dynamics (also termed stochastic rotation dynamics).[17,18] In this model solvent positions and momenta evolve through free streaming and effective collisions in a manner that preserves mass, momentum, and energy. As a result, a hydrodynamic description emerges on long distance and time scales. The solvent model can be combined with full molecular dynamics to simulate the dynamics of solute molecules dissolved in the solvent.[19] In this hybrid MD-MPC dynamics hydrodynamic interactions among the solute molecules are automatically taken into account.[20,21]

The aims of this paper are to demonstrate that the hybrid MD-MPC dynamics can be used effectively to study polymer dynamics in solution under varying good and poor solvent conditions and to obtain information on polymer collapse dynamics and polymer frictional properties for different solvents. MPC dynamics has already been used to study several aspects of polymer dynamics.[22–28] In contrast to these studies, we model interactions between the polymer beads and mesoscopic solvent molecules by intermolecular forces that mimic both good and poor solvents. The introduction of explicit polymer bead-solvent particle intermolecular forces in the hybrid MD-MPC method, while computationally more demanding than schemes which use MPC dynamics for both solvent-solvent and solvent-bead interactions, has the advantages that solvent particles can no longer freely stream through the polymer and the solvent structure in the immediate vicinity of the polymer arising from bead-solvent interactions is taken into account. While computations of equilibrium properties of a polymer under varying solvent

---

[a)] Electronic mail: shlee@ks.ac.kr
[b)] Electronic mail: rkapral@chem.utoronto.ca

conditions can be carried out using effective potentials (of mean force) between polymer beads, the treatment of both equilibrium and dynamical properties requires a consistent formulation of the equations of motion. Simulations based on MPC dynamics may be contrasted with Langevin schemes where explicit solvent phase space coordinates are projected out of the dynamics. The solvent is then accounted for by effective potential-of-mean-force interactions among the polymer beads and frictional and random forces on the beads. The effective potentials can be obtained by integrating out the solvent configurations to determine the free energy as a function of bead coordinates while configuration-dependent friction tensors must be supplied as input into such Langevin models to account approximately for hydrodynamic interactions.

The outline of the paper is as follows. In Sec. II we describe the polymer and solvent models used in this investigation of polymer dynamics. Section III describes the dynamics following a sudden change from good to poor solvent conditions and presents results on the structure of the collapsed polymer for different bead-solvent interaction potentials. In addition, this section also discusses the dynamics following a sudden change from poor to good solvent conditions. Frictional properties are topic of Sec. IV. The collapse dynamics and structure of block copolymers are described in Sec. V, while Sec. VI contains the conclusions of the study.

II. POLYMER AND SOLVENT MODELS

We consider a standard bead-spring model of a linear polymer chain with N_b beads and suppose that the polymer is in a solution containing of N_s molecules. The Hamiltonian of the system consists of the sum of the kinetic energies of all bead and solvent molecules and the total potential energy $V(\mathbf{r}^{N_b},\mathbf{r}^{N_s})$ of the system. In our mesoscopic model the total potential energy consists of contributions arising from interactions among the polymer beads, $V_{bb}(\mathbf{r}^{N_b})$, and bead-solvent interactions, $\mathbf{V}_{bs}(\mathbf{r}^{N_b},\mathbf{r}^{N_s})$. Interactions among the solvent molecules are accounted for by multiparticle collisions as discussed below.

The interactions among the polymer beads consist of bead-spring potentials between neighboring beads as well as bead-bead interactions among all beads. The non-Hookian bead-spring potential[29,30] is given by finite extensible nonlinear elastic (FENE) interactions,

$$V_{\mathrm{FENE}}(r) = -\frac{\kappa}{2}R_0^2 \ln\left[1-\left(\frac{r}{R_0}\right)^2\right], \quad r < R_0, \tag{1}$$

where $\kappa=30\epsilon/\sigma^2$ and $R_0=1.5\sigma$.

Two types of bead-bead interactions among all beads are considered: (A) Attractive Lennard-Jones (LJ) interactions,

$$V_{\mathrm{LJ}}(r) = 4\epsilon\left[\left(\frac{\sigma}{r}\right)^{12} - \left(\frac{\sigma}{r}\right)^{6}\right]. \tag{2}$$

The LJ potentials are cut off at a distance $L/4$ where L is the length of simulation box (52.9868σ). (B) Repulsive LJ interactions,[31]

$$V_{\mathrm{LJ}}^{R}(r) = \begin{cases} 4\epsilon[(\sigma/r)^{12} - (\sigma/r)^{6} + (1/4)], & r \leqslant r_c \\ 0, & r > r_c, \end{cases} \tag{3}$$

are also studied where $r_c=2^{1/6}\sigma$.

Since the solvent bath in which the polymer dynamics takes place must contain a very large number of molecules to account properly for solvation and collective hydrodynamic effects, instead of using full molecular dynamics to describe the solvent motions, we utilize a mesoscopic multiparticle collision description of the solvent dynamics.[17] In the MPC model, no intermolecular forces act among the solvent molecules, instead, interactions are accounted for by collisions that take place at discrete time intervals τ. The system volume is partitioned into n^3 cells given labels ξ and at each time τ rotation operators $\hat{\omega}_\xi$, chosen at random from set of rotation operators, are assigned to each cell. We take rotations by $\pm\pi/2$ about a randomly chosen axis, but other choices are possible.

At any chosen time, a cell will contain a number of solvent molecules with velocities $\mathbf{v}_i'$. Let V_ξ be the center of mass velocity of the particles in cell ξ. The postcollision velocities of the particles in the cell are determined by rotating the particle velocities, relative to the center of mass velocity V_ξ, by the rotation operator $\hat{\omega}_\xi$, and then adding V_ξ to the result,

$$\mathbf{v}_i = \mathsf{V}_\xi + \hat{\omega}_\xi[\mathbf{v}_i' - \mathsf{V}_\xi]. \tag{4}$$

These multiparticle collisions take place independently in each cell. Between multiparticle collisions solvent molecules move under the influence of solvent-bead intermolecular forces. The combination of multiparticle collisions and streaming motion specify the mesoscopic MPC solvent dynamics. Random shifting of the grid used to define the multiparticle collision volumes[32–34] was implemented in our simulations.

MPC dynamics conserves mass, momentum, and energy, phase space volumes are preserved, and the equilibrium single particle velocity distribution is a Maxwell-Boltzmann distribution. Starting from MPC dynamics, one may derive the hydrodynamic equations and transport coefficients of the model.[17–19,35] This mesoscopic model has proven its utility in a variety of applications (see, for example, Ref. 18 and references therein). It goes beyond simple Langevin descriptions of the solvent dynamics since it shares the basic conservation and phase space volume preservation properties with full molecular dynamics. Consequently, frictional properties and hydrodynamic interactions, crucial for a proper description of polymer dynamics in solution, follow automatically from the dynamics and need not be supplied as input to the calculation.

Finally, we must specify the interactions between the polymer beads and the solvent molecules. These are also taken to be of either the attractive or repulsive type. The attractive LJ interactions have the form

$$V_{bs}(r)=\begin{cases} cV_{\rm LJ}(r), & r\leq r_t \\ cV_{\rm LJ}(r)S(r), & r_t<r\leq r_c \\ 0, & r>r_c, \end{cases} \tag{5}$$

and are cut off at a short distance with a switching function,[36] $S(r)=1-[(r-r_t)^2(3r_c-2r-r_t)/(r_c-r_t)^3]$, that acts between $r_t=1.1688\sigma$ and $r_c=1.3636\sigma$. The LJ parameter c in this equation is used to scale ϵ and takes the values $c=1/12$ and $1/3$ to model weak and strong bead-solvent attractive forces. The repulsive LJ bead-solvent interactions have the same form as the repulsive bead-bead interactions given above.

The full dynamics of the polymer in the presence of the solvent is then carried out using the hybrid MPC-MD dynamics.[19] Newton's equations of motion are solved to evolve the polymer taking into account the forces derived from the bead-spring, bead-bead, and bead-solvent interactions. Since there are no solvent-solvent interactions these do not appear in the equations of motion. However, at time intervals τ multiparticle collisions as described above take place and the evolution is continued. This hybrid dynamics again conserves mass momentum and energy and preserves phase space volumes.

A. Simulation details

Using the model described above, we have carried simulations of the dynamics of a system containing N_s mesoscopic solvent particles of mass m and one polymer with N_b beads of mass $M=10m$. We present results for N_b=40, 60, 100, and 200 beads. The simulations were carried out in a cubic box of volume $V=L^3$ with periodic boundary conditions. If the volume of the bead particle is $V_b=\frac{4}{3}\pi\sigma^3$, V_0 is defined as the volume of the system occupied by solvent molecules, $V_0=V-N_bV_b$. The multiparticle collision cell volume is given by $V_\xi=V/n^3=(L/n)^3=\ell^3$. We have taken $n=32$. The values of L and N_s were chosen to fix the number density of solvent particles at $\rho_s=N_s/V_0=2.2027\ \sigma^{-3}$ or an average of ten particles per collision cell so that there are 327 680 solvent molecules in the simulation box.

We use dimensionless LJ units throughout the paper where distances are measured in units of σ, energy in units of ϵ, time in units of $\sigma\sqrt{m/\epsilon}$, and temperature in units of ϵ/k_B. Newton's equations of motion were integrated using the velocity Verlet algorithm,[37] with a time step of $\Delta t=0.016\,56$. Multiparticle solvent collisions were carried out in cells with linear dimension $\ell=L/n$ every 100 molecular-dynamics time steps so that $\tau=100\Delta t$. The temperature was determined from the average kinetic energy and, unless otherwise stated, was taken to be $T=1/3$. The results were obtained from ensembles of ten microcanonical MD trajectories of length approximately 1.66×10^5 time units.

III. POLYMER DYNAMICS AND STRUCTURE

The systems we consider may be classified according to the nature of the bead-bead (b-b) and bead-solvent (b-s) interactions. Letting upper case symbols **A** and **R** denote attractive and repulsive b-b interactions and lower case symbols **a** and **r** denote attractive and repulsive b-s interactions, the various polymer-solvent systems will be designated as **Ii** where **I**=**A**,**R** and **i**=**a**,**r**. A system with **Ra** interactions mimics a polymer with repulsive bead-bead interactions in good solvent. For **i**=**a**, the weak bead-solvent attractive force ($c=1/12$) was employed, unless otherwise stated. For **Ra** interactions the polymer exists in an expanded state as shown in the upper left panel of Fig. 1. In all other cases, **Aa**, **Rr**, and **Ar**, the polymer exists in a collapsed form with the **Aa** system having the least compact polymer structure and the polymer with **Ar** interactions being most compact.

FIG. 1. Polymer collapse starting from a polymer (N_b=200) with repulsive bead-bead interactions in a good solvent with attractive bead-solvent interactions (**Ra**) (top left panel) following a sudden change to attractive bead-bead interactions in a poor solvent with repulsive bead-solvent interactions (**Ar**) resulting in a fully collapsed polymer (bottom right panel). The end beads in the polymer chain are distinguished by a different shading. The solvent molecules are not shown. The polymer configurations shown in the panels correspond to times t=0.0, 15.6, 33.7, 90.9, 138.3, and 827.0, from left to right and top to bottom, respectively.

A. Polymer collapse

As an illustration, we consider the collapse dynamics when the potential for the **Ra** system is changed suddenly to **Ar** interactions, modeling a polymer with attractive bead-bead forces in a poor solvent with repulsive bead-solvent interactions. Collapse occurs as shown in the series of panels in Fig. 1. The final state of the **Ar** polymer is a compact elongated structure. In this and subsequent figures the end beads are distinguished by a different shading from other beads in the chain. One can see that the free ends of the polymer chain tend to reside at the ends of the long axis of the elongated collapsed polymer, consistent with the larger conformational freedom associated with such configurations compared to configurations where the free ends reside in the interior of the collapsed polymer.[38–43]

Our investigations of polymer collapse were carried out on relatively small chains with N_b=40–200. As a result some aspects of the proposed mechanisms for collapse, especially scaling predictions, cannot be analyzed on the basis of our simulation results. Nevertheless, our simulations are consistent with many of the basic elements in theoretical models of the collapse.[6–9] In particular, our results show that the collapse from the expanded state proceeds as follows (see Fig. 1): first "blobs" of polymer beads are formed where

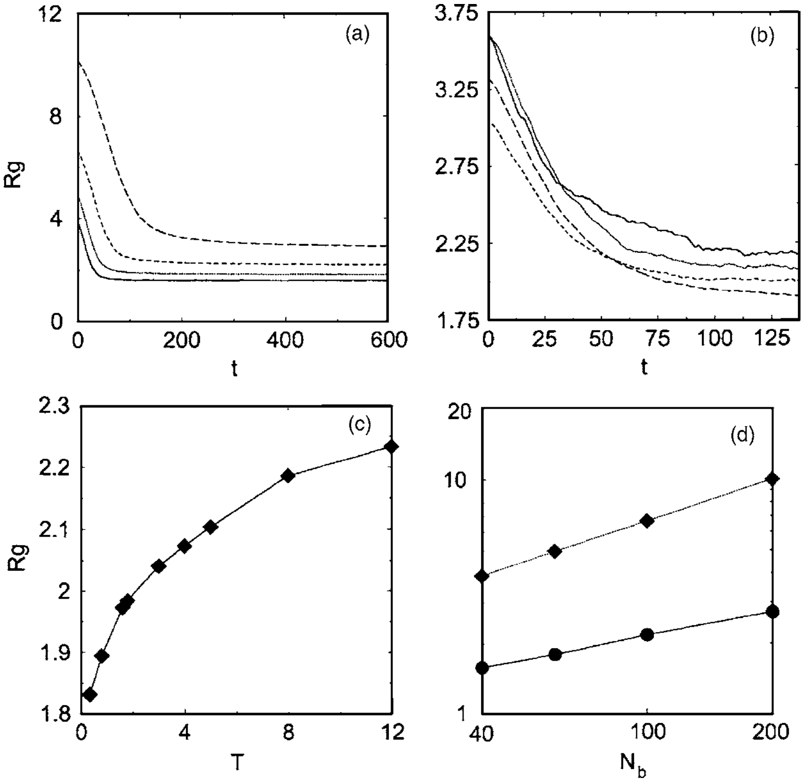

FIG. 2. Plots of Rg vs time for (a) several values of N_b, from bottom, N_b=40, 60, 100, and 200 for $T=1/3$ (b) several values of the temperature T, from top, T=12.0, 5.0, 1.6, and 0.333, for N_b=60. The lower panels show (c) $\overline{Rg}$ vs T for N_b=60 and (d) a log-log plot of $\overline{Rg}$ vs N_b for $T=1/3$ for **Ar** (circles) and **Ra** (diamonds). The slopes of the curves in (d) are approximately 0.34 and 0.58, respectively.

portions of the chain are in close proximity, separated by segments of the uncollapsed chain. As time progresses, the blobs coalesce to form a thick sausage-shaped structure, which continues to thicken and shrink until the collapsed elongated polymer state is reached.

The collapse dynamics can be analyzed by computing the time variation of the radius of gyration $Rg(t)$, averaged over several realizations of the collapse dynamics starting from different configurations of the expanded polymer. Here $Rg^2(t)=N_b^{-1}\Sigma_{i=1}^{N_b}|(\mathbf{r}_i(t)-\mathbf{r}_{\mathrm{CM}}(t))|^2$, where $\mathbf{r}_i$ is the position of bead i and $\mathbf{r}_{\mathrm{CM}}$ is the center of mass of the polymer chain. This data is summarized in Fig. 2 which shows plots of (a) $Rg(t)$ versus time for several values of N_b, (b) for $N_b=60$ and various values of the temperature T, (c) $\overline{Rg}$ versus T for $N_b=60$, where $\overline{Rg}$ is the average asymptotic value of Rg, and (d) a log-log plot of $\overline{Rg}$ versus N_b for $T=1/3$. The results confirm several anticipated trends: the polymer collapses more slowly as the polymer length increases and the temperature decreases. If the collapse time is defined as the time τ for which $Rg(\tau)=\overline{Rg}+(Rg(0)-\overline{Rg})/20$,[28] our results [Fig. 3 (left panel)] for the **Ra**→**Ar** collapse show that the collapse time increases linearly with N_b which is consistent with the predictions of a model of the collapse that involves a fast formation of blobs along the chain followed by a slower compaction of the chain.[44] Our simulation results can be fit by $\tau(N_b)=13.2+1.07N_b$ for fixed $T=1/3$. The right panel of this figure shows that τ decreases with increasing temperature as expected. The size of the collapsed polymer, as reflected in the average asymptotic value $\overline{Rg}$, increases with increasing temperature and N_b [see Fig. 2(c)]. From the log-log plot in (d) we find $\overline{Rg}\sim N_b^{\nu}$, with an exponent $\nu\approx 0.34$ for the **Ar** system which is close to the value $\nu=1/3$ expected for a polymer chain collapsed into a dense globule[2] and $\nu\approx 0.58$ for the **Ra** system which is close to the value $\nu\approx 0.588$ expected for a swollen chain in a good solvent.[45–47]

The structure of the collapsed polymer with **Ar** parameters can be studied by computing the radial distribution functions for polymer and solvent molecules relative to the center of mass of the polymer. These distributions are defined as

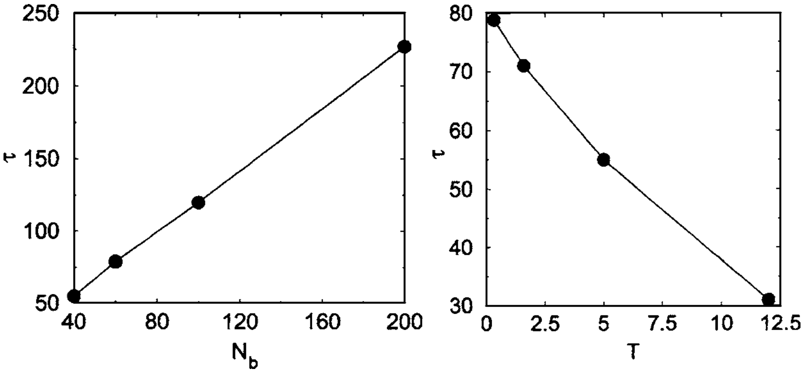

FIG. 3. Plots of the collapse time τ vs (left) N_b for $T=1/3$ and (right) T for N_b=60.

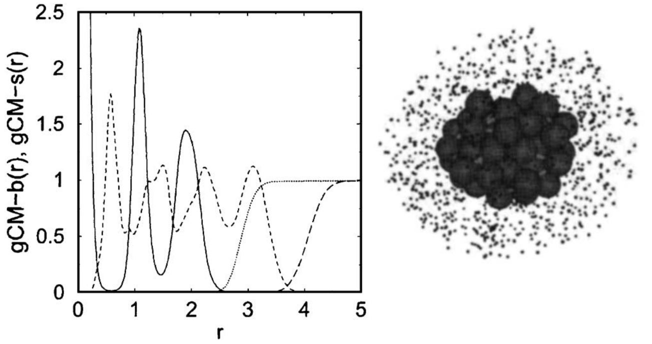

FIG. 4. (left) Radial distribution functions $g_{\mathrm{CM}-b}(r)$ (solid line and short dashed line) and $g_{\mathrm{CM}-s}(r)$ (dotted line and long dashed line) vs r for $N_b=60$ and 200, respectively. (right) Final collapsed state of an **Ar** polymer with $N_b=60$ showing neighboring solvent molecules which do not penetrate into the interior of the collapsed polymer.

$$g_{\mathrm{CM}-\nu}(r)=\frac{1}{4\pi r^2\rho_\nu}\left\langle\sum_i^{N_\nu}\delta(|\mathbf{r}_i-\mathbf{r}_{\mathrm{CM}}|-r)\right\rangle, \tag{6}$$

where $\nu=b$ or s labels a polymer or solvent molecule and ρ_ν is the number density of polymer bead or solvent molecules. Figure 4 shows the radial distribution functions for polymers with $N_b=60$ and 200 beads. The radius of the polymer r_p can be estimated from the radial distribution functions and was found to be $r_p\approx 1.95$, 2.24, 2.73, and 3.41 for polymers with $N_b=40$, 60, 100, and 200, respectively. However, recall that the asymptotic collapsed polymer is not spherical (see Fig. 1) and the radial distribution results reflect the average over all orientations. For polymer chains with **Ar** interactions the deviations from sphericity of the collapsed polymer are not great. The asphericity can be measured by $\langle A\rangle=\langle\frac{1}{2}[(R_1^2-R_2^2)^2+(R_1^2-R_3^2)^2+(R_2^2-R_3^2)^2]\rangle/\langle(R_1^2+R_2^2+R_3^2)^2\rangle$, where the R_i^2 are the three principle radii of gyration squared of the polymer chain. The asyphericity parameter $\langle A\rangle$ varies from zero for spherically symmetrical polymer chains and tends to unity for very elongated chains.[41] We find $\langle A\rangle=0.0087$, 0.0032, 0.0028, and 0.0016 for $N_b=40$, 60, 100, and 200, respectively. The decrease with increasing N_b can be attributed to the smaller fluctuations for the larger polymer chains.

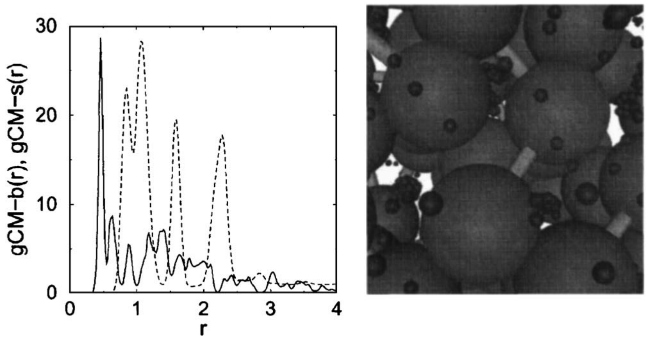

FIG. 5. (left) Plots of the radial distribution functions for the polymer beads (solid line) and solvent molecules (dashed line) for **Aa** interactions with $c=1/3$ and $N_b=60$ indicating the structure of the trapped solvent in the interior of the collapsed polymer. The polymer bead radial distribution function has been scaled by a factor of 14 to more easily compare the results. (right) A view of the interior of the collapsed polymer showing trapped solvent molecules.

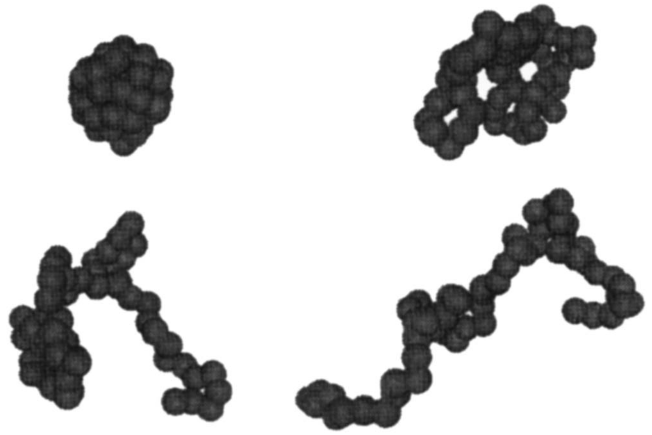

FIG. 6. Expansion of the polymer from the collapsed state following the parameter change **Ar**→**Ra**. Time increases from left to right and top to bottom.

Figure 4 also shows the structural ordering of the beads within the collapsed polymer. Furthermore, we see that the solvent is excluded from the collapsed polymer. From the nature of the collapse dynamics described above, the polymer chain gradually excludes solvent from its interior as small blobs of the collapsed chain are formed. As these blobs coalesce and the chain thickens into a sausage shape, solvent is continually pushed out of compact regions of the chain. Consequently, for the solvent conditions in this simulation, with attractive bead-bead interactions and repulsive bead-solvent interactions, there is little opportunity for solvent to become trapped in the interior of the collapsed chain.

Solvent can penetrate into the collapsed polymer for other bead-solvent interactions. For **Aa** interactions with $c=1/3$, the solvent penetrates into the collapsed polymer as seen in Fig. 5. From the structure of the radial distribution function, and an examination of the interior of the collapsed polymer (right panel), one can see that the trapped solvent has a highly structured configuration that follows the structural ordering of the polymer beads. If the attractive interaction strength is changed to $c=1/12$, the solvent is excluded from the polymer.

B. Polymer expansion

We can also consider polymer dynamics when the system parameters are changed from those corresponding to a

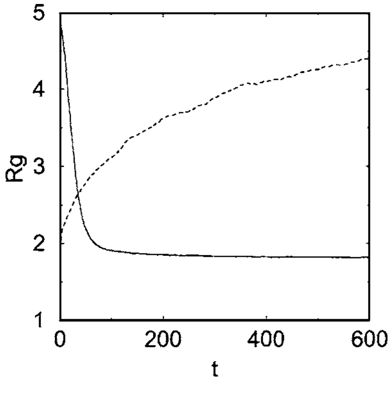

FIG. 7. $Rg(t)$ vs t for expanding and collapsing polymers with $N_b=60$ monomer beads.

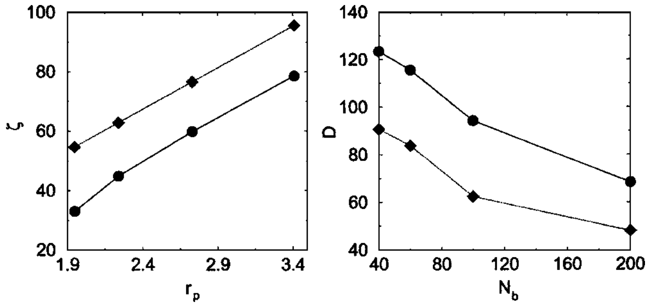

FIG. 8. (left) The friction coefficients ζ_p (●) and ζ^S (◆) as function of radius of cluster, r_p. (right) Diffusion coefficients ($\times 10^4$) of moving polymers as function of number of beads, N_b, obtained from mean-square displacement (●), and $D=k_BT/\zeta$ with ζ taken from the simulation (◆).

collapsed polymer in a poor solvent to those for an expanded polymer in a good solvent. In particular, we consider the parameter change **Ar**→**Ra**, the reverse of that discussed above. Figure 6 shows several polymer configurations during the course of the expansion process. Figure 7 plots the radius of gyration versus time in such a process and compares the time evolution with the collapse dynamics. The fact that the collapse and expansion curves have very different forms is expected in view of the strongly nonequilibrium nature of the dynamics following the sudden changes in the interaction potentials that characterize the systems.

IV. FRICTIONAL PROPERTIES

The time-dependent friction coefficient for a polymer is defined in terms of the finite-time integral of the autocorrelation function of the force on the center of mass of the polymer,

$$\zeta(t) = \frac{\beta}{3}\int_0^t dt' \langle \mathbf{f}_{\mathrm{CM}}^p(0)\cdot \mathbf{f}_{\mathrm{CM}}^p(t')\rangle_0, \tag{7}$$

where $\mathbf{f}_{\mathrm{CM}}^p=\mathbf{F}_{\mathrm{CM}}^p-\langle \mathbf{F}_{\mathrm{CM}}^p\rangle_0$ with $\mathbf{F}_{\mathrm{CM}}^p$ the total force on the polymer center of mass, $\mathbf{F}_{\mathrm{CM}}^p=\Sigma_{i=1}^{N_b}\mathbf{F}_i$, where $\mathbf{F}_i$ is the force on bead i. The angular brackets denote a canonical equilibrium average with the center of mass of the polymer fixed. In our calculations of the friction, the center of mass of the polymer was fixed by a holonomic constraint.[48] The friction coefficient ζ is defined as $\lim_{t\to\infty}\zeta(t)$. The force on a polymer bead i is $\mathbf{F}_i=-\partial V(\mathbf{r}^{N_b},\mathbf{r}^{N_s})/\partial \mathbf{r}_i=-\partial V_{bb}(\mathbf{r}^{N_b})/\partial \mathbf{r}_i-\partial V_{bs}(\mathbf{r}^{N_b},\mathbf{r}^{N_s})/\partial \mathbf{r}_i$, so that the total force on the polymer center of mass arises solely from bead-solvent interactions, $\mathbf{F}_{\mathrm{CM}}^p=-\Sigma_{i=1}^{N_b}\partial V_{bs}(\mathbf{r}^{N_b},\mathbf{r}^{N_s})/\partial \mathbf{r}_i$, since the net force from bead-bead interactions vanishes. Thus, the friction coefficient is determined by bead-solvent force correlations.

The simulation of the friction coefficient is a subtle problem requiring long simulations on large systems, even for a single spherical particle in solution[20] or for pairs of spherical particles where hydrodynamic interactions between the particles come into play.[21] We consider the frictional properties of the system with **Ar** interactions where the polymer is in its most collapsed form and solvent does not penetrate into the interior of the collapsed polymer. Figure 8 (left panel) plots the friction coefficients for various values of the polymer radius r_p. The polymer radius was determined from the radial distribution function. For large radii, the friction coefficient of the polymer increases approximately linearly with radius of polymer, a signature of the dominance of collective solvent effects on the friction.[49] For **Ar** interactions the collapsed polymer is compact and can be crudely approximated by a sphere with an effective radius. The central LJ bead-solvent forces, since they act at the polymer bead-solvent particle level, macroscopically give rise to effective stick boundary conditions. Consequently, we may compare the simulation results with the Stokes law form of the friction coefficient of a sphere of radius r_p interacting through stick boundary conditions with a continuum medium with viscosity η: $\zeta^S=6\pi\eta r_p$. The solvent viscosity was determined from a simulation of the stress-stress autocorrelation functions and was found to be[20] $\eta=1.49$. In the figure we also plot ζ^S vs r_p and we can see that it does not provide a quantitatively accurate estimate of the friction. This discrepancy likely arises from the fact that the simple Stokes law form fails to capture the internal dynamics of the polymer chain and the hydrodynamic interactions among the polymer beads, especially those on the surface of the collapsed polymer. In addition, the mesoscopic treatment of the solvent approximately accounts for the presence of a boundary layer in the vicinity of the polymer beads. This effect is absent when the solvent is treated as a continuum fluid. Finite size effects arising from periodic boundary conditions will also affect the simulated friction coefficients.

The diffusion coefficient D of the polymer was also computed from both the mean-square displacement and center of mass velocity autocorrelation function, which yielded similar values for D. The results are presented in Fig. 8 (right panel) and show, as expected, that D falls as N_b increases. The figure also compares the values of D obtained from these simulations with the Stokes-Einstein formula, $D=k_BT/\zeta$, for a single spherical particle. The friction coefficient was determined from the force autocorrelation function calculation described above. The results show that while this formula yields a similar variation with N_b to the mean-square displacement simulation, it underestimates the value of the diffusion coefficient.

V. BLOCK COPOLYMER COLLAPSE

Next, we consider some aspects of the collapse dynamics and structure of block copolymers in order to illustrate some of the new phenomena that arise as a result of different bead-solvent interactions within the same polymer. We focus on block copolymers composed to two types of monomer units, labeled A and B, which interact differently with the solvent molecules. The block lengths are denoted by N_A and N_B. We refer to such block copolymers by **Ah** or **Rh**, depending on whether the bead-bead interaction is attractive or repulsive. The results presented earlier showed that for **Aa**, **Ar**, and **Rr** interactions the polymer exists in a collapsed form while for **Ra** interactions the polymer is in an expanded form. Consequently, block copolymers with mixtures of these interactions should show distinctive dynamics and structure.

Consider block copolymers of the form AB composed of

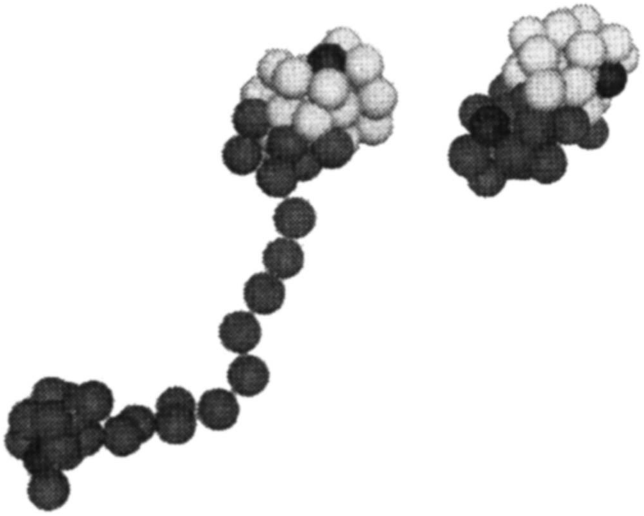

FIG. 9. (left) Intermediate state of an *AB* block copolymer with $N_A = N_B = 30$ and $N_b = N_A + N_B = 60$ and attractive bead-bead interactions and half attractive and half repulsive bead-solvent interactions (**Ah**). (right) Final collapsed state of the polymer showing the dumbbell form where the two blocks are segregated.

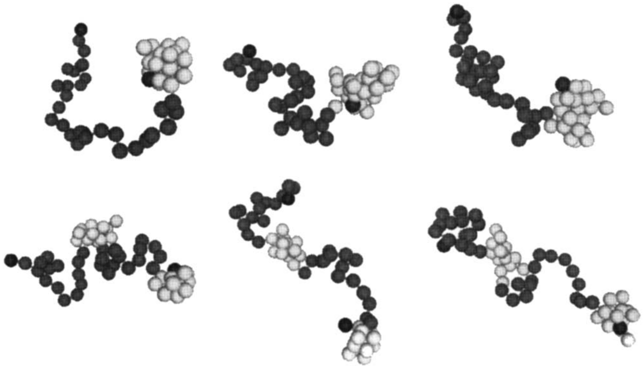

FIG. 10. **Rh** repulsive bead-bead interactions and half attractive and half repulsive bead-solvent interactions: (top) Several equilibrium conformations of the an *AB* block copolymer with $N_A = N_B = 30$, and $N_b = N_A + N_B = 60$. (bottom) Equilibrium conformations of an *ABAB* block copolymer with $N_A = N_B = 15$ and $N_b = 2N_A + 2N_B = 60$.

two blocks with $N_A = N_B$ with **Ah** interactions. Since the interactions for each of the blocks, **Aa** and **Ar**, correspond to polymers that exist in collapsed forms, we expect that the *AB* copolymer will also exist in a collapsed form. This is indeed the case but both the dynamics and equilibrium structure exhibit differences from the homopolymer case. Pictures of polymer configurations are shown in Fig. 9. For the homopolymer, relaxation to the collapsed state occurs more rapidly for a system with **Ar** interactions than that for a system with **Aa** interactions and leads to a more compact form of the collapsed polymer. As Fig. 9 (left panel) shows, at intermediate times during the collapse dynamics the block with **Ar** interactions has already collapsed while the block with **Aa** interactions has not yet collapsed. Finally a fully collapsed state is reached (right panel) but the copolymer adopts a dumbbell shape consisting of two collapsed portions which do not mix. Differences in the bead-solvent interactions are sufficient to produce this phase segregation.

While a homopolymer with **Rr** interactions exists in a collapsed state, one with **Ra** interactions is in an expanded state. An *AB* block copolymer with **Rh** interactions composed of blocks of equal length exhibits both of these features and its equilibrium form consists of a collapsed portion attached to tail of expanded polymer [see Fig. 10 (top panel)]. The figure shows several conformations of the equilibrium state of the polymer chain. This structure also manifests itself in *ABAB* block copolymers with blocks of equal length of alternating *A*- and *B*-type monomers. Several conformations of equilibrium structures are shown in Fig. 10 (bottom panel). We see that there are alternating compact and expanded segments of the polymer chain.

VI. CONCLUSIONS

The results presented in this paper showed that the hybrid MD-MPC simulation scheme can be used to explore a variety of polymer dynamical properties. Earlier investigations[22–24,26–28] have already shown that many aspects of polymer dynamics can be studied using MPC dynamics, especially those that depend on hydrodynamic interactions. In the MD-MPC algorithm employed in this investigation, the polymer beads interact with the mesoscopic solvent molecules through intermolecular forces. Consequently, by modifying the nature of these interactions, the character of the solvation structure of the polymer could be changed. In particular, the quality of the solvent could be altered from good to varying levels of poor solvent conditions. In poor solvents the degree of compactness of the polymer could be varied and solvent could either be excluded from the interior of the polymer chain or be present in the interior of the chain more fully solvating the polymer beads. The studies of block copolymers showed how specific solvent interactions can have especially pronounced effects on both the structure and collapse dynamics of polymers.

Specific solvent characteristics influence the collapse dynamics of the polymer chain when solvent conditions are suddenly changed. The fact that the MPC solvent dynamics conserves momentum means that the dynamics automatically accounts for hydrodynamic interactions among the beads, which is crucial for determining both the time scale and mechanism of the chain collapse. These hydrodynamic interactions also play an essential role in determining the values of the frictional properties of the polymer solution.

The hybrid MD-MPC model involves additional computational demands since full MD that includes all bead-bead and bead-solvent interactions between multiparticle solvent collisions must be carried out. However, the simulations are still highly efficient since no solvent-solvent interactions need be computed by MD and the number of solvent molecules employed in the simulations is orders of magnitude greater than the number of polymer beads. Thus, the model should find use in applications where specific solvent effects on polymer dynamics and structure need to be taken into account.

ACKNOWLEDGMENTS

The work of one of the authors (S.H.L.) was supported by the Korea Research Foundation Grant funded by the Korean Government (MOEHRD) (KRF-2005-041-C00210). The work of one of the authors (R.K.) was supported in part by a grant from the Natural Sciences and Engineering Research Council of Canada. We would like to thank S. G. Whittington for numerous useful discussions in the course of this work.

[1] H. Yamakawa, *Modern Theory of Polymer Solutions* (Harper & Row, New York, 1971).

[2] P.-G. de Gennes, *Scaling Concepts in Polymer Physics* (Cornell University Press, Ithaca, 1988).

[3] M. Doi and S. F. Edwards, *Theory of Polymer Solutions* (Clarendon, Oxford, 1989).

[4] A. Yu. Grosberg and A. R. Kohkhlov, *Statistical Mechanics of Macromolecules* (AIP, New York, 1994).

[5] W. H. Stockmayer, Macromol. Chem. Phys. **35**, 54 (1960).

[6] P.-G. de Gennes, J. Phys. (France) Lett. **46**, L639 (1985).

[7] A. Yu. Grosberg, S. K. Nechaey, and E. I. Shakhnovich, J. Phys. (France) **49**, 2095 (1988).

[8] A. Halperin and P. M. Goldbart, Phys. Rev. E **61**, 565 (2000).

[9] L. I. Klushin, J. Chem. Phys. **108**, 7917 (1998).

[10] R. Brak, A. J. Guttmann, and S. G. Whittington, J. Phys. A **25**, 2437 (1992).

[11] E. G. Timoshenko and K. A. Dawson, Phys. Rev. E **51**, 492 (1995).

[12] E. Pitard and H. Orland, Europhys. Lett. **41**, 467 (1998).

[13] A. Montesi, M. Pasquali, and F. C. MacKintosh, Phys. Rev. E **69**, 021916 (2004).

[14] R. Chang and Y. Yethiraj, J. Chem. Phys. **114**, 7688 (2001).

[15] J. Polson and M. Zuckermann, J. Chem. Phys. **113**, 1283 (2000).

[16] J. Polson and M. Zuckermann, J. Chem. Phys. **116**, 7244 (2002).

[17] A. Malevanets and R. Kapral, J. Chem. Phys. **110**, 8605 (1999).

[18] A. Malevanets and R. Kapral, Lect. Notes Phys. **640**, 116 (2004).

[19] A. Malevanets and R. Kapral, J. Chem. Phys. **112**, 7260 (2000).

[20] S. H. Lee and R. Kapral, J. Chem. Phys. **121**, 11163 (2004).

[21] S. H. Lee and R. Kapral, J. Chem. Phys. **122**, 214916 (2005).

[22] M. Ripoll, K. Mussawisade, R. G. Winkler, and G. Gompper, Europhys. Lett. **68**, 106 (2004).

[23] R. G. Winkler, K. Mussawisade, M. Ripoll, and G. Gompper, J. Phys.: Condens. Matter **16**, S3941 (2004).

[24] R. G. Winkler, M. Ripoll, K. Mussawisade, and G. Gompper, Comput. Phys. Commun. **169**, 326 (2005).

[25] K. Mussawisade, M. Ripoll, R. G. Winkler, and G. Gompper, J. Chem. Phys. **123**, 144905 (2005).

[26] A. Malevanets and J. M. Yeomans, Europhys. Lett. **52**, 231 (2000).

[27] I. Ali, D. Marenduzzo, and J. M. Yeomans, J. Chem. Phys. **121**, 8635 (2004).

[28] N. Kikuchi, A. Gent, and J. M. Yeomans, Eur. Phys. J. E **9**, 63 (2002).

[29] R. B. Bird, C. F. Curtiss, R. C. Armstrong, and O. Hassager, *Dynamics of Polymeric Liquids* (Wiley, New York, 1987).

[30] K. Kremer and G. Grest, J. Chem. Phys. **92**, 5057 (1990).

[31] D. Frenkel and B. Smit, in *Understanding Molecular Simulation*, 2nd ed. (Academic, San Diego, 2001).

[32] T. Ihle and D. M. Kroll, Phys. Rev. E **63**, 020201 (2001).

[33] A. Lamura, G. Gompper, T. Ihle, and D. M. Kroll, Europhys. Lett. **56**, 768 (2001).

[34] A. Lamura, G. Gompper, T. Ihle, and D. M. Kroll, Europhys. Lett. **56**, 319 (2001).

[35] N. Kikuchi, C. M. Pooley, J. F. Ryder, and J. M. Yeomans, J. Chem. Phys. **119**, 6388 (2003).

[36] O. Steinhauser, Mol. Phys. **45**, 335 (1982).

[37] W. C. Swope, H. C. Andersen, P. H. Berens, and K. R. Wilson, J. Chem. Phys. **76**, 673 (1982).

[38] W. Kuhn, Kolloid-Z. **68**, 2 (1934).

[39] W. Gobush, W. Solc, and W. H. Stockmayer, J. Chem. Phys. **60**, 12 (1974).

[40] D. E. Kranbuehl and P. H. Verdier, J. Chem. Phys. **67**, 361 (1977).

[41] J. Rudnick and G. Gaspari, J. Phys. A **19**, L191 (1986).

[42] F. Fougere and J. Desbois, J. Phys. A **26**, 7253 (1993).

[43] C. Haber, S. A. Ruiz, and D. Wirtz, Proc. Natl. Acad. Sci. U.S.A. **97**, 10792 (2000).

[44] A. Buguin, F. Brochard-Wyart, and P. G. de Gennes, C. R. Acad. Sci. Paris, Ser II b **322**, 741 (1996).

[45] J. C. Le Guillou and J. Zinn-Justin, J. Phys. (France) **50**, 1365 (1989).

[46] B. Li, N. Madras, and A. D. Sokal, J. Stat. Phys. **80**, 661 (1995).

[47] S. Caracciolo, M. S. Causo, and A. Pelissetto, J. Chem. Phys. **112**, 7693 (2000).

[48] J. P. Ryckaert, G. Ciccotti, and H. J. Berendsen, J. Comput. Phys. **23**, 327 (1977).

[49] J. T. Hynes, R. Kapral, and M. Weinberg, J. Chem. Phys. **70**, 1456 (1970).